$$i \propto P_{O_2}[H^+]^{3/2} \exp\left(-\frac{FV}{RT}\right) \quad [20]$$

This equation has a Tafel slope of RT/F, and has the correct oxygen partial pressure and pH-dependence (11).

Acknowledgment

The author wishes to thank Pratt & Whitney Aircraft Division of United Aircraft Corporation, and the sponsors of this work under the TARGET fuel cell program, for permission to publish this paper. The help of the various members of IGT who assisted in preparation is also greatly appreciated.

Manuscript submitted Aug. 1, 1969; revised manuscript received *ca.* Nov. 12, 1969.

Any discussion of this paper will appear in a Discussion Section to be published in the December 1970 JOURNAL.

REFERENCES

1. D. T. Sawyer and L. V. Interrante, *J. Electroanal. Chem.*, **2**, 310 (1961).
2. M. W. Breiter, *Electrochim. Acta*, **9**, 441 (1964).
3. C. C. Liang and A. L. Juliard, *J. Electroanal. Chem.*, **9**, 390 (1965).
4. E. I. Khrushcheva, N. A. Shumilova, and M. R. Tarasevich, *Elektrokhim.*, **1**, 730 (1965).
5. L. Müller and L. N. Nekrasov, *Dokl. Akad. Nauk. S.S.S.R.*, **157**, 416 (1964).
6. L. Müller and L. N. Nekrasov, *J. Electroanal. Chem.*, **9**, 282 (1965).
7. J. P. Hoare, *This Journal*, **112**, 602 (1965).
8. G. Bianchi and T. Mussini, *Electrochim. Acta*, **10**, 445 (1965).
9. J. J. Lingane, *J. Electroanal. Chem.*, **2**, 296 (1961).
10. A. Damjanovic and J. O'M. Bockris, *Electrochim. Acta*, **11**, 376 (1966).
11. A. Damjanovic and V. Brusic, *ibid.*, **12**, 615 (1967).
12. A. Damjanovic, A. Dey, and J. O'M. Bockris, *ibid.*, **11**, 791 (1966).
13. A. Damjanovic, M. A. Genshaw, and J. O'M. Bockris, *This Journal*, **114**, 466 (1967).
14. A. Damjanovic, M. A. Genshaw, and J. O'M. Bockris, *J. Chem. Phys.*, **45**, 4057 (1966).
15. A. J. Appleby, *J. Electroanal. Chem.*, **24**, 97 (1970).
16. H. A. Laitenen and C. G. Enke, *This Journal*, **107**, 773 (1960).
17. A. K. N. Reddy, M. Genshaw, and J. O'M. Bockris, *J. Electroanal. Chem.*, **8**, 406 (1964).
18. S. D. James, *This Journal*, **114**, 1113 (1967).
19. S. Schuldiner and T. B. Warner, *ibid.*, **112**, 212 (1966).
20. J. P. Hoare, *ibid.*, **109**, 858 (1962).
21. H. Wroblowa, M. L. B. Rao, A. Damjanovic, and J. O'M. Bockris, *J. Electroanal. Chem.*, **15**, 139 (1967).
22. G. Lewis and M. Randell, "Thermodynamics and Free Energy of Chemical Substances," McGraw-Hill Book Co., New York (1923).
23. Monsanto Corporation, Technical Bulletin *1-239*.
24. J. Bravacos, M. Bonnemay, E. Levart, and A. A. Pilla, *Compt. Rend. Acad. Sci. Paris*, **265**, 337 (1967).
25. A. J. Appleby and A. Borucka, *This Journal*, **116**, 1212 (1969).
26. V. S. Bagotskii and I. E. Yablokova, *Z. Fiz. Khim.*, **27**, 1663 (1953).
27. L. Müller and L. N. Nekrasov, *Dokl. Akad. Nauk. SSSR*, **154**, 437 (1964).
28. L. Müller and V. V. Sobol, *Elektrokhim.*, **1**, 111 (1965).
29. L. N. Nekrasov, *ibid.*, **2**, 438 (1966).
30. H. P. Stout, *Discussions Faraday Soc.*, **1**, 246 (1947).
31. A. C. Riddiford, *Electrochim. Acta*, **4**, 170 (1961).
32. T. P. Hoar, *Proc. 8th Meeting CITCE, Madrid 1956*, p. 439, Butterworths, London (1958).
33. H. Mauser, *Z. Elektrochem.*, **62**, 419 (1958).
34. D. S. Gnanamuthu and J. V. Petrocelli, *This Journal*, **114**, 1036 (1967).
35. J. O'M. Bockris, *J. Chem. Phys.*, **24**, 817 (1956).
36. B. E. Conway and P. L. Bourgault, *Can. J. Chem.*, **40**, 1690 (1962).
37. D. J. Ives and G. J. Janz, "Reference Electrodes—Theory and Practice," p. 365, Academic Press, New York (1961).
38. J. P. Hoare, *This Journal*, **112**, 849 (1965).
39. B. E. Conway and E. Gileadi, *Trans. Faraday Soc.*, **58**, 2493 (1962).
40. W. Böld and M. Breiter, *Electrochim. Acta*, **5**, 145 (1961).
41. O. A. Petrii, R. V. Marvet, and Zh. N. Malysheva, *Elektrokhim.*, **3**, 962 (1967).
42. R. Parsons, *Trans. Faraday Soc.*, **54**, 1053 (1958).
43. T. Biegler and R. Woods, *J. Electroanal. Chem.*, **20**, 347 (1969).
44. A. Damjanovic, Private communication (1969).

Rotating Ring-Disk Electrodes

II. Digital Simulation of First and Second-Order Following Chemical Reactions

Keith B. Prater[1] and Allen J. Bard*

Department of Chemistry, The University of Texas at Austin, Austin, Texas

ABSTRACT

A digital simulation technique has been employed to treat the steady-state and transient ring current behavior at the rotating ring-disk electrode (RRDE) for cases where the intermediate generated at the disk electrode undergoes a first- or second-order homogeneous chemical reaction leading to a nonelectroactive species. Where comparisons were possible, the results were found to be in good agreement with previous approximate theoretical treatments. Working curves are provided which allow determination of rate constants of the homogeneous reactions from ring-current-rotation rate data.

The rotating ring-disk electrode (RRDE) was introduced by Frumkin and Nekrasov (1) as a means of detecting intermediates of electrode reactions. An intermediate, B, is generated at the disk electrode by the reaction

$$A \pm ne \rightarrow B \quad [1]$$

and B is detected at the ring electrode by applying a sufficient potential such that all B reaching the ring is transformed back to A by the reaction

$$B \pm ne \rightarrow A \quad [2]$$

If B is a stable species, then the ratio of the current at the ring electrode to the current at the disk electrode is a function only of the geometry of the electrode (2). This ratio is called the collection efficiency, N, and is given by the expression

[1] Present address: University of Texas at El Paso, El Paso, Texas.
* Electrochemical Society Active Member.

$$N = -i_r/i_d \quad [3]$$

If species B undergoes a chemical reaction which depletes its concentration as it passes from the disk to the ring, then the observed collection efficiency under these conditions, N_k, (the kinetic collection efficiency) will be smaller than that found in the absence of these reactions. In this case, the collection efficiency is a function, not only of electrode geometry, but also of the rate constant of the reaction, the rotation rate, ω, and other solution parameters.

Albery and Bruckenstein (3) have given an approximate treatment of steady-state kinetic collection efficiencies for the first-order EC mechanism (where EC denotes an electron transfer followed by a chemical reaction)

$$B \xrightarrow{k_1} X \quad [4]$$

in which B reacts to give an electro-inactive species X. This treatment is valid only for extremely thin-ring thin-gap electrodes and then only for certain values of k_1/ω. In a later paper, Albery, Hitchman, and Ulstrup (4) modified the previous treatment to make it applicable to a wider range of electrode geometries. Albery (5) has also treated the ring current transients for this mechanism in the case of a constant current at the disk electrode.

Albery and Bruckenstein (6) have also given an approximate treatment of the second-order EC mechanism

$$B + C \xrightarrow{k_2} Y + Z \quad [5]$$

where C, Y, and Z are electro-inactive species. Unfortunately, the treatment of this mechanism is valid only for very small values of the parameter $k_2C^\circ_A/\omega$ where C°_A is the bulk concentration of species A.

Albery, Hitchman, and Ulstrup (4) have presented experimental work to support the modified treatment of the first-order case, and Johnson and Bruckenstein (7) have investigated the second-order case. In both of these studies, however, the systems chosen did not strictly conform to the above mechanisms in that in all cases one product of the homogeneous following reaction was the starting species, A. Thus, the experimental studies were more related to the catalytic reaction mechanism; a theoretical treatment of that case will be given in a later paper.

In this paper, we present the results of the application of a digital simulation technique (8) to the first- and second-order EC mechanisms. In addition to steady-state kinetic collection efficiencies, ring current transient behavior is presented. This simulation technique can be applied to any electrode and the results are valid for any value of the rate parameters, k_1/ω and $k_2C^\circ_A/\omega$.

Digital Simulation Method

The basic method for the digital simulation of the RRDE including the simulation of the first-order EC mechanism has been presented in a previous paper (8). Only two modifications of the simulation technique previously presented are necessary in order to simulate the second-order EC mechanism. First, the collection efficiency for such a process will be determined not only by the value of the rate constant, k_2, the rotation rate, ω, and the bulk concentration of species C, C°_C. For the second-order case, then, an additional parameter, m, given by

$$m = C^\circ_C/C^\circ_A \quad [6]$$

must be specified. Thus in setting up the initial conditions, the fractional concentration of species A in any box will be

$$F_A(J,K) = 1.0 \quad [7]$$

and the initial fractional concentration of species C in any box will be

$$F_C(J,K) = m \quad [8]$$

A second difference between the treatment of the first- and second-order cases concerns the form of the dimensionless rate parameter. The pertinent rate law for the second-order mechanism is

$$-dC_C/dt = -dC_B/dt = k_2C_BC_C \quad [9]$$

In terms of the simulation this becomes

$$-\Delta C_C = -\Delta C_B = k_2C_BC_C\Delta t \quad [10]$$

Dividing through by C°_A and letting

$$C_C/C^\circ_A = F_C \quad [11]$$

and

$$C_B/C^\circ_A = F_B \quad [12]$$

then Eq. [10] becomes

$$-\Delta F_C = -\Delta F_B = k_2F_BC_C\Delta t \quad [13]$$

Replacing C_C by $F_CC^\circ_A$ and using the equation (Eq. [12] and [25], ref. (8))

$$\Delta t = t_k/L = \nu^{1/3}D_A^{-1/3}\omega^{-1}L^{-1}(0.51)^{-2/3} \quad [14]$$

one obtains

$$-\Delta F_C = -\Delta F_B = k_2t_kC^\circ_AF_BF_C/L \quad [15]$$

The product $k_2t_kC^\circ_A$ is the dimensionless rate parameter applicable to this mechanism and is called XKTC. Thus

$$XKTC = k_2t_kC^\circ_A = k_2C^\circ_A\omega^{-1}\nu^{1/3}D_A^{-1/3}(0.51)^{-2/3} \quad [16]$$

where as before ν is the kinematic viscosity and D_A is the diffusion coefficient of species A.

The effects of kinetics on the concentration in any box may be taken into account by replacing the existing concentrations of B and C, F_B and F_C by

$$F'_B(J,K) = F_B(J,K) - \Delta F_B(J,K) \quad [17]$$

$$F'_C(J,K) = F_C(J,K) - \Delta F_C(J,K) \quad [18]$$

Other than these two modifications, the simulation is identical to that previously presented.

A digital computer program based on the digital simulation model with the appropriate modifications was used to obtain the results which will be presented. These results were obtained by first selecting a value for the appropriate dimensionless rate parameter

$$XKT = (0.51)^{-2/3}k_1\omega^{-1}\nu^{-1/3}D_A^{-1/3} \quad [19]$$

for the first-order case or XKTC for the second-order case. In the second-order case, a value for the parameter m was also specified. The computation was then carried out until a steady state was attained. This computation yields both steady-state kinetic collection efficiencies, N_K, and the ring current transients as functions of the dimensionless rate parameters and m. In all cases unless otherwise stated, $L = 50$ and $D_m = 0.45$ and the appropriate correction factors were used.

First-Order Results

Steady-state behavior.—The simulated collection efficiency *vs.* XKT curve for an electrode approximating the thin-ring thin-gap electrode treated by Albery and Bruckenstein is shown in Fig. 1 and 2. In Fig. 1, the simulation is compared with Albery and Bruckenstein's Eq. [6.4] (3) in the region of small XKT. The entire simulated curve is shown in Fig. 2 as is the comparison with their Eq. [5.8] (3). These graphs show clearly the regions in which the approximate treatments of Albery and Bruckenstein apply for an electrode of this geometry. These regions of applicability are quite close to those suggested by Albery and Bruckenstein.

In a later paper (4), Albery pointed out that the thin-ring thin-gap treatment is not valid for most

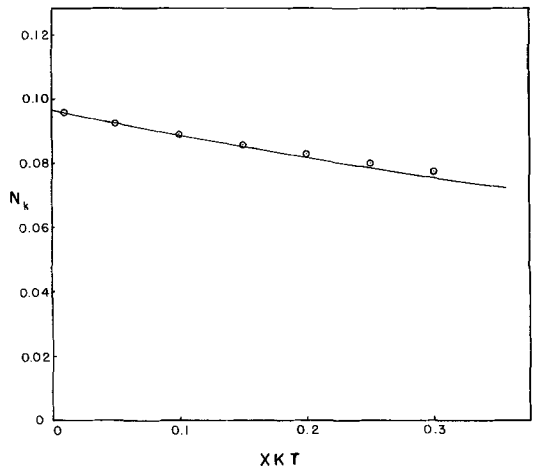

Fig. 1. Collection efficiency vs. XKT for a first-order following reaction at a thin-ring thin-gap electrode (IR1 = 2000, IR2 = 2040, IR3 = 2080). ⊙ Comparison with Albery's Eq. [6.4] (2). XKT = $k_1\omega^{-1}D^{-1/3}\upsilon^{1/3}(0.51)^{-2/3}$.

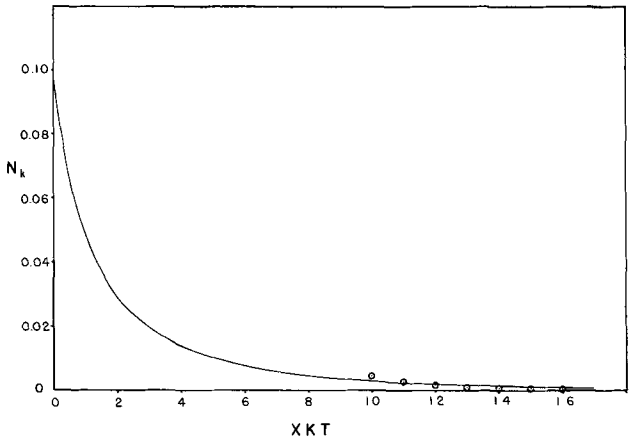

Fig. 2. Collection efficiency vs. XKT for a first-order following reaction at thin-ring thin-gap electrode (IR1 = 2000, IR2 = 2040, IR3 = 2080). ⊙ Comparison with Albery's Eq. [5.8] (2). XKT = $k_1\omega^{-1}D^{-1/3}\nu^{1/3}(0.51)^{-2/3}$.

practical electrodes, and he presented a modified theory which should be applicable to a wider range of electrode geometries. The results of the simulation of the two electrodes for which Albery presented his calculations are shown in Fig. 3 as well as Albery's calculated values for the collection efficiency as a function of $(XKT)^{1/2}$. The agreement over this range of XKT values is excellent.

It is interesting to consider the effect of electrode geometry on the range of applicability of different electrodes to studies of first-order following reactions. The results of the simulation of three different electrodes are given in Fig. 4. Electrode A is the electrode previously presented which approximates the thin-ring thin-gap electrode. Electrode B is one of Albery's electrodes. It has a fairly thin gap and a moderately thin ring. Electrode C which has been used in these laboratories has a comparatively wide gap and ring. The simulated working curves show, as expected, that the thin-ring thin-gap electrode (A) is the most applicable of the three for studying extremely fast reactions, while electrode C, with a wider gap is more useful for slow reactions. The point to be made here is that while electrodes similar to electrode A should be used for studying fast reactions, they are not useful for slow reactions ($k \leq 0.1$) because even at the lowest usable rotation rates such a reaction does not proceed to any detectable extent in the time required for species B to reach the ring electrode. In these cases, electrodes with gaps as wide as that in electrode C or even wider should be used

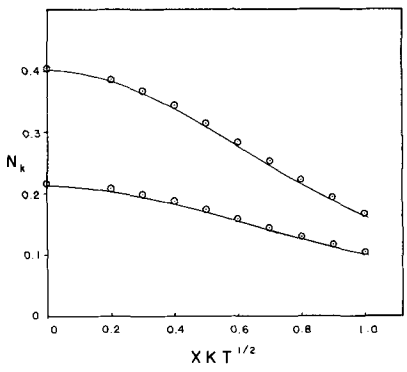

Fig. 3. Collection efficiency vs. $(XKT)^{1/2}$ for a first-order following reaction for two electrodes of different geometries

a. $r_1 = 0.3635$	$r_2 = 0.3777$	$r_3 = 0.4835$
IR1 = 200	IR2 = 208	IR3 = 266
b. $r_1 = 0.4770$	$r_2 = 0.4869$	$r_3 = 0.5222$
IR1 = 820	IR2 = 837	IR3 = 898

⊙ Comparison with Albery's Fig. 2 (4). XKT = $k_1\omega^{-1}D^{-1/3}\upsilon^{1/3}(0.51)^{-2/3}$.

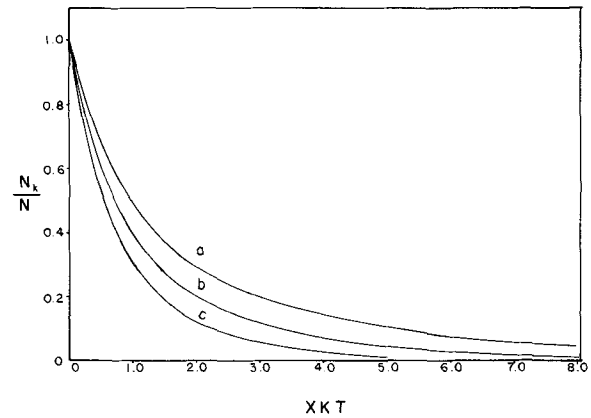

Fig. 4. Collection efficiency vs. XKT for a first-order following reaction for three electrodes of different geometries. XKT = $k_1\omega^{-1}D^{-1/3}\upsilon^{1/3}(0.51)^{-2/3}$. a, $r_2/r_1 = 1.02$, $r_3/r_2 = 1.02$; b, $r_2/r_1 = 1.04$, $r_3/r_2 = 1.28$; c, $r_2/r_1 = 1.14$, $r_3/r_2 = 1.70$.

For this first-order case, identical steady-state collection efficiencies are predicted when the boundary condition at the disk electrode corresponds to a constant current step instead of a potential step. The constant current boundary condition at the disk affects only the transient and not the steady-state behavior of the collection efficiency.

Transient behavior.—The simulated ring current transients (RCT) for this mechanism due to a potential step at the disk are shown in Fig. 5. Each curve represents the RCT for the specified value of the dimensionless rate parameter, XKT. As must be the case, the steady-state currents are seen to decrease with increasing values of XKT. An interesting feature of these curves is that, unlike the RCT in the absence of a following reaction, the ring current passes through a maximum before attaining steady state. This is because under the potential step condition, a very large instantaneous flux of species B is generated at the initiation of electrolysis [see Fig. 2, ref. (8)]. The short time interval between the generation of this large flux of B and the detection of B at the ring does not permit the homogeneous reaction to reduce the concentration of B to its eventual, lower steady-state value. Hence a maximum in the ring current is observed. Identical simulation results are obtained if the simulation is carried out with L = 1000 and no correction factors. This effect is more clearly shown in

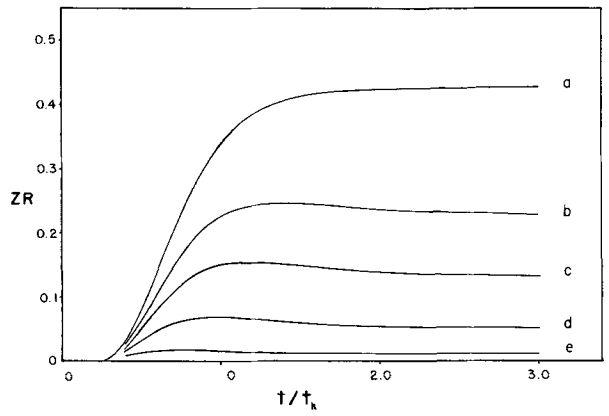

Fig. 5. Ring current transients for a first-order following reaction for different values of XKT. a, 0.0; b, 0.5; c, 1.0; d, 2.0; e, 4.0. Zr $= i_r/(0.51)^{1/3}nFA_DC^\circ{}_AD_B^{2/3}\omega^{1/2}\upsilon^{-1/6}$. XKT $= k_1\omega^{-1}D^{-1/3}\upsilon^{1/3}(0.51)^{-2/3}$. Simulated with IR1 = 83, IR2 = 94, IR3 = 159.

Fig. 6 in which the RCT's have each been normalized by the eventual steady-state current for each value of XKT. This plot also points out that the value of $\omega t\ D^{1/3}\nu^{-1/3}(0.51)^{2/3}$ at which the ring current is one-half (or any other fraction) of the steady-state value is a function of XKT and could in principle be used to determine the rate constant, as has been suggested by Albery (5).

These results can be compared with those obtained using a constant current boundary condition at the disk. The results of two simulations which differed only in the boundary condition at the disk are shown in Fig. 7. Note that no maximum is observed when a constant current is applied to the disk. The effect of the rate parameter on the normalized RCT's with a constant current step at the disk is shown in Fig. 8. As before, the value of the time parameter, $\omega t\ D^{1/3}\nu^{-1/3}(0.51)^{2/3}$, at a specified fraction of the steady-state current is a function of the rate parameter, XKT. It should also be pointed out that these normalized curves are independent of the value of the applied constant current.

Second-Order Results

Steady-state behavior.—A series of curves of N_k *vs.* (XKTC) (m) for different values of m, for a following second-order reaction and for the disk electrode held at a potential where the limiting current for the conversion of A to B occurs, is shown in Fig. 9. Also shown in Fig. 9 is the simulated collection efficiency

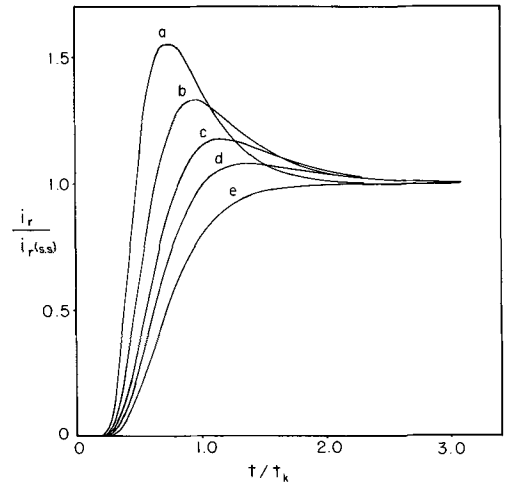

Fig. 6. Ring current transients for a first-order following reaction for different values of XKT. a, 4.0; b, 2.0; c, 1.0; d, 0.5; e, 0.0. Curves are normalized by the steady-state current at each value of XKT. Simulated for IR1 = 83, IR2 = 94, IR3 = 159. XKT $= k_1\omega^{-1}D^{-1/3}\upsilon^{1/3}(0.51)^{-2/3}$.

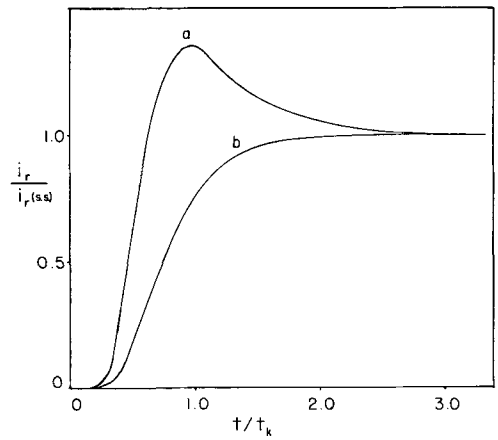

Fig. 7. Ring current transients for a first-order following reaction for XKT = 2.0, IR1 = 83, IR2 = 94, IR3 = 159. $t_k = \omega^{-1}D^{-1/3}\upsilon^{1/3}(0.51)^{-2/3}$. a, Potential step at the disk electrode; b, constant current at the disk electrode.

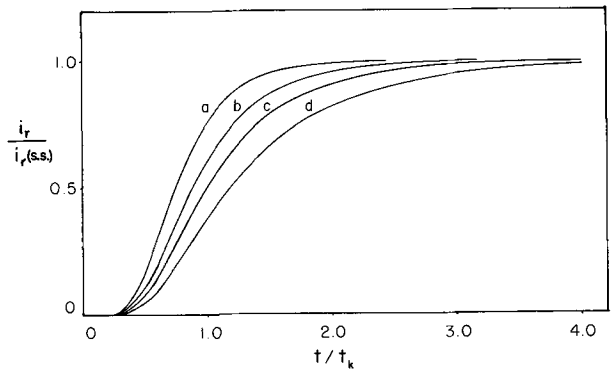

Fig. 8. Ring current transients for a first-order following reaction with constant current at the disk for different values of XKT. $t_k = \omega^{-1}D^{-1/3}\upsilon^{1/3}(0.51)^{-2/3}$. a, 2.0; b, 1.0; c, 0.5; d, 0.0. IR1 = 83, IR2 = 94, IR3 = 159.

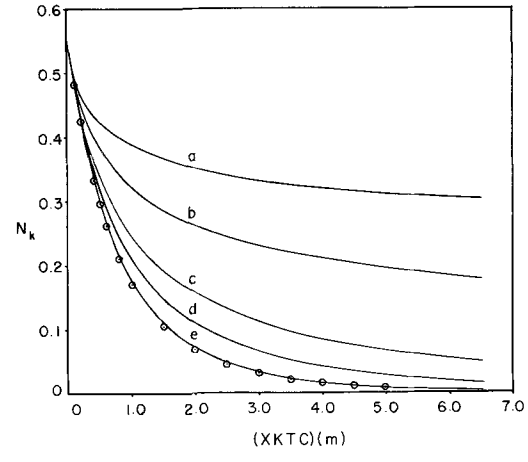

Fig. 9. Collection efficiency *vs.* (XKTC)(m) for a second-order following reaction for different values of m $= C^\circ_C/C^\circ_A$. a, 0.10; b, 0.20; c, 0.50; d, 1.0; e, 10.0. ⊙ Simulated first-order curve. IR1 = 83, IR2 = 94, IR3 = 159. XKTC $= k_2\omega^{-1}C^\circ{}_AD^{-1/3}\upsilon^{1/3}(0.51)^{-2/3}$.

curve for a first-order following reaction. Note that when C is in tenfold excess, the second-order curve is almost indistinguishable from the first-order curve; thus when m = 10.0, the second-order process can be treated as a pseudo-first-order one.

In the case of this second-order mechanism, unlike that of a following first-order reaction, the simulated collection efficiencies presented here are valid only for the case $i_d = i_{lim}$. If a constant current less than the limiting current were applied to the disk, differ-

ent collection efficiencies would be observed as pointed out by Albery and Bruckenstein (6). The simulation of the effects of a constant current less than the limiting current can easily be done, but there seems to be little reason to do so.

In the treatment of this case by Albery and Bruckenstein (6), the current at the disk electrode is adjusted to a value where the concentrations of B and C are equal at the inner edge of the ring electrode. Under these conditions, the current at the ring due to species B will be dependent on the rate of the reaction between B and C and is given by the following equation

$$i_r = BnF\pi r_2^2 D_A \omega^{3/2} \nu^{-1/2} k_2^{-1} \quad [20]$$

The constant, B, was originally calculated to be 590 (6) but more recently has been given as 210 (7). The disk current necessary to produce the appropriate conditions is given by

$$i_d = 620nF\pi r_1^2 D_A^{2/3} \omega^{1/2} \nu^{-1/6} C^\circ_C (1 - F(\alpha))^{-1} \quad [21]$$

where $F(\alpha)$ is a geometrical parameter of the electrode which has been tabulated by Albery and Bruckenstein (2). Note that for the particular value of m, given by

$$m = C^\circ_C / C^\circ_A = 1 - F(\alpha) \quad [22]$$

Eq. [21] becomes

$$i_d = 620nF\pi r_1^2 D_A^{2/3} \omega^{1/2} \nu^{-1/6} C^\circ_A \quad [23]$$

This is precisely the limiting current due to species A as predicted by the Levich equation. Thus from Eq. [20] and [23], N_k in this case is given by

$$N_k = (B/620)(r_2/r_1)^2 \omega k_2^{-1} C^\circ_A{}^{-1} D^{1/3} \nu^{-1/3} \quad [24]$$

or

$$N_k = (B/620)(r_2/r_1)^2 (0.51)^{2/3} (XKTC)^{-1} \quad [25]$$

Note that Eq. [24] must at best be valid only as $\omega/k_2 C^\circ_A$ approaches zero where it accurately predicts that, under these conditions, N_k approaches zero. At the other limit, as $\omega/k_2 C^\circ_A$ approaches infinity, Eq. [24] predicts that N_k should increase without bound, while in reality the actual upper limit is N, the collection efficiency in the absence of kinetic complications.

To compare the digital simulation results with those of Albery and Bruckenstein (6), an electrode of a given geometry was chosen, and m was adjusted according to Eq. [22]. Values of N_k at various values of XKTC with i_d at its limiting value can then be used to investigate the useful range of Eq. [24].

Simulated collection efficiencies *vs.* 1/XKTC are shown in Fig. 10 for one of Albery's electrodes under these conditions. Also shown is the line predicted by Eq. [25] using B = 210. The simulation yields curves which approach the proper limits (zero or N) for the extreme values of $\omega/k_2 C^\circ_A$. In the region of small $\omega/k_2 C^\circ_A$, the simulated curve is approximately linear, but the agreement with Eq. [25] depends on the particular geometry. The slope of the simulated curve as $\omega/k_2 C^\circ_A$ approaches zero yields a value of B of about 260, but it seems that the use of the entire simulated working curve would be preferable to an approximate linearization near $\omega/k_2 C^\circ_A = 0$.

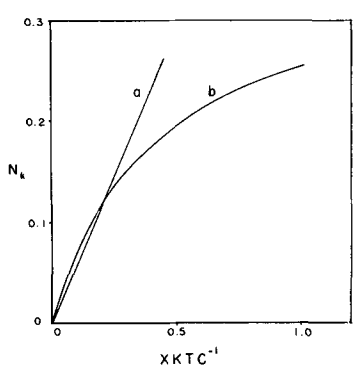

Fig. 10. Collection efficiency *vs.* $(XKTC)^{-1}$ for a second-order following reaction. m = 0.60. IR1 = 200, IR2 = 208, IR3 = 266. XKTC = $k_2\omega^{-1}C^\circ_A D^{-1/3}\upsilon^{1/3}$ $(0.51)^{-2/3}$. Curve a is a plot of Eq. [25]; curve b is the simulated curve.

Albery and Bruckenstein's recommended experimental procedure involves variation of i_d at values below the limiting current and at constant ω to obtain the i_r values used in fitting Eq. [24]. It appears that a more straight forward procedure when working curves such as those in Fig. 9 are available, would involve maintaining i_d at its limiting value and studying the variation of N_k with ω and m. The value of k_2 is then obtained by fitting the experimental results to these working curves.

Transient behavior.—A description of RCT's for second-order following reactions has not been given previously. The simulation shows that the RCT's for the second-order mechanism are similar to those for the first-order case. As shown in Fig. 11, the extent to which a maximum is predicted in the potential step case is a function of the ratio of the bulk concentrations of species A and C. If A is in excess, then the maximum is small because very little B disappears on its way to the ring and the RCT approaches the RCT in the absence of a following reaction. If C is in excess, then the maxima are similar to those obtained for the first-order case.

Conclusion

The digital simulation technique is capable of describing both the steady-state and transient behavior at the RRDE for systems involving homogeneous reactions following the electrode reaction for a wide range of electrode geometries, ω and R. Although the simulation technique permits the calculation of the transient behavior of the ring current, there are many experimental problems involved in measuring these transients. The most important problem is that adsorption of the intermediate, B, on the disk electrode will delay and smear out the RCT while desorption of B produced from adsorbed A will produce a maximum similar in form to the one predicted for this kinetic case, even in the absence of kinetic effects. Bruckenstein (9) has considered cases like this and their effects on transients. Since adsorption of either product or reactant is so frequently found, the observation of the maxima predicted by the simulation will be difficult. For the same reason, the use of RRDE transient measurements to investigate the kinetics of homogeneous reactions is probably less profitable and more difficult, than the corresponding steady-state measure-

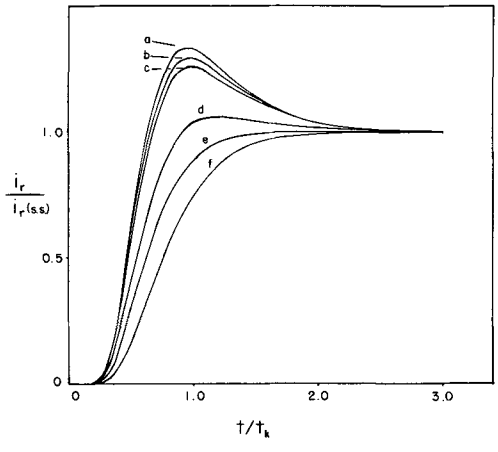

Fig. 11. Ring current transients for a second-order following reaction with a potential step at the disk. $t_k = \omega^{-1}D^{-1/3}\upsilon^{1/3}(0.51)^{-2/3}$. IR1 = 83. IR2 = 94, IR3 = 159. The curves are all generated for (XKTC)(m) = 2.0 at different values of m; also shown is the first-order curve. a, First-order; b, 10.0; c, 5.0; d, 1.0; e, 0.5; f, 0.1.

ments. We might point out that adsorption interferes in a similar way in other types of electrochemical transient measurements (*e.g.*, cyclic voltammetry and chronopotentiometry).

The method of obtaining rate constants proposed here involves setting the disk current at its limiting value, observing the ring current as a function of ω, and fitting the results to working curves for the particular RRDE employed. This technique should prove just as useful, and operationally somewhat easier, than the technique suggested by Albery and Bruckenstein (6). The relatively small value of m which yields essentially pseudo-first-order behavior ($m > 10$) suggests that a good fit to the first-order working curves does not necessarily indicate that a second-order reaction is not involved.

Acknowledgment

The support of the Mobil Oil Corporation and the Eastman Kodak Company for fellowships to one of us (K.B.P.) and the Robert A. Welch Foundation and National Science Foundation (GP 6688X) are gratefully acknowledged. The authors are indebted to J. T. Maloy for helpful discussions during the course of this work.

Manuscript submitted May 29, 1969; revised manuscript received *ca.* Nov. 17, 1969.

Any discussion of this paper will appear in a Discussion Section to be published in the December 1970 JOURNAL.

REFERENCES

1. A. N. Frumkin and L. N. Nekrasov, *Doklady Akad. Nauk. SSSR*, **126**, 115 (1959).
2. W. J. Albery and S. Bruckenstein, *Trans. Faraday Soc.*, **62**, 1920 (1966).
3. W. J. Albery and S. Bruckenstein, *ibid.*, 1946 (1966).
4. W. J. Albery, M. L. Hitchman, and J. Ulstrup, *ibid.*, **64**, 2831 (1968).
5. W. J. Albery, *ibid.*, **63**, 1771 (1967).
6. W. J. Albery and S. Bruckenstein, *ibid.*, **62**, 2584 (1966).
7. D. C. Johnson and S. Bruckenstein, *J. Am. Chem. Soc.*, **90**, 6592 (1968).
8. K. B. Prater and A. J. Bard, *This Journal*, **117**, 207 (1970).
9. S. Bruckenstein and D. T. Napp, *J. Am. Chem. Soc.*, **90**, 6303 (1968).

Technical Notes

Ultrafine Porous Polymer Membranes as Battery Separators

Joseph L. Weininger* and Fred F. Holub

General Electric Research and Development Center, Schenectady, New York

In nonaqueous galvanic systems, based on organic solvents, it is important to keep soluble ions of the cathodic reactant from the anode. Conventional ion exchange membranes have been used (1, 2) for this purpose, but have not been able to support appreciable current densities. In solvent exchange only an insufficient amount of organic solvent, *e.g.* propylene carbonate or dimethyl sulfoxide, replaces water in the ion exchange resin. To obviate this problem and obtain a separator for organic electrolyte cells, an alternate method of ion exclusion is reported in this note.

It is possible to restrict migration of solvated ions by reducing the pore size of microporous membranes below a certain limit. Different methods are known of producing microporous polymers by the introduction of additives into a thermoplastic resin and following this by the removal of the additive to leave a porous structure. For example, Sargent and Safford (3) introduced anionic surfactants into polyethylene and processed the mixture. After the additive is leached out, there remains a microporous structure. Similarly, in the present method ultrafine porous polymer membranes are prepared. These membranes are flexible, about 50% porous, and, most importantly, have extremely fine pore size. The average pore size is between 40 and 120Å.

Membranes were prepared by adding sodium benzoate or other salts of benzoic acid to the melted polymer in a weight ratio of 70-85 parts of benzoate to 30-15 parts of polymer. The salt does not dissolve in the polymer, but forms a dispersion or colloidal suspension. In processing, the polymer was milled on differential rolls with the benzoate salt at 140°-160°C for polyethylene or 170°-180°C for polypropylene. The mixtures were then cooled close to the softening point of the polymer and sheeted into 0.005-in. thick films. The final leaching of the sheets occurred in water at 20°-55°C. The salt was generally extracted in 1-16 hr. However, leaching is almost complete within 5-10 min.

In some cases the polymers were also irradiated with high energy electrons of 20 Mr at a dose rate of 10 Mr/min before or after extraction of the salt. This irradiation step was employed to improve the thermal and mechanical properties of the porous polymer for possible later use at greater than ambient pressures and temperatures. Irradiation after leaching was more effective in strengthening mechanical and thermal properties, but by this treatment the smallest pores were closed by cross-linking.

Membranes were tested routinely for porosity, gas permeability, and electrolytic conductivity. The porosity was determined by density measurements, the gas permeability from nitrogen flow as a function of applied pressure, and the electrolytic conductivity was measured at 1 kHz with a conductance bridge after filling the membrane with 1M KCl.

The known porosity of 40-50% corresponds to the initial weight ratio of polymer and additive. The conductivity is of the same order of magnitude as that of the solution filling the membrane. This shows an open continuous pore structure. Finally, small gas permeability is a measure of small pore diameters.

From the magnitude of the conductivity, a tortuosity factor can be calculated. It is the ratio of the actual electrolytic conductance to that expected at the given porosity and thickness for a structure with straight pores, normal to the surfaces.

The properties of three membranes are listed in Table I. They are given as examples of the magnitudes

* Electrochemical Society Active Member.